Li^+ Ion Insertion in TiO_2 (Anatase). 1. Chronoamperometry on CVD Films and Nanoporous Films

Henrik Lindström, Sven Södergren, Anita Solbrand, Håkan Rensmo, Johan Hjelm, Anders Hagfeldt,* and Sten-Eric Lindquist*

Department of Physical Chemistry, University of Uppsala, Box 532, S-75121, Uppsala, Sweden

Received: February 6, 1997; In Final Form: July 9, 1997[⊗]

Electrochemical insertion of lithium in nanoporous and CVD samples of TiO_2 (anatase) was studied by chronoamperometry. The currents following cathodic and anodic potential steps were monitored as a function of film thickness, temperature, and electrolyte concentration. The time dependence of the currents generally exhibit the behavior of a diffusion-limited process. It is demonstrated that the magnitude of the currents scales directly with the inner area of the electrodes. The potential dependence on the rate of insertion and extraction indicates that the reduction of Ti^{4+} and oxidation of Ti^{3+} is kinetically hindered. The double-layer capacitance and the adsorbate concentration at 0 V of the nanoporous structure were determined to be 30−40 μF/cm^2 and 1.7−2.4 mol/cm^2, respectively. The chemical diffusion coefficient at 25 °C for insertion and extraction in the nanoporous structure was 1×10^{-17} and 4×10^{-17} cm^2/s, respectively. The corresponding values for the CVD samples, using the projected area, were 2×10^{-15} cm^2/s for insertion and 6×10^{-15} cm^2/s for extraction. The activation energy for lithium insertion and extraction was 0.35 and 0.38 eV for the nanoporous films and 0.54 and 0.78 eV for the CVD samples.

1. Introduction

The electrochemical process in which cations are incorporated into the bulk lattice of a solid electrode is termed ion intercalation or ion insertion. The chemical diffusion coefficient for the solid state mass transfer of these cations[1] is commonly used as a quality parameter in the determination of the response time in device applications including batteries, displays, and smart windows. To calculate the chemical diffusion coefficient, parameters such as the electrode area, the film thickness, and the concentration gradient of the diffusing species must be invoked. Due to the difficulty in determining the active electrode area accurately (e.g., for sputtered, evaporated, or CVD samples), the apparent diffusion coefficients are as a common rule calculated by using the outer or projected electrode area. The drawback of this procedure is the problem of performing comparative studies of the intrinsic material properties. Indeed, the diffusion coefficients might differ several orders of magnitude using merely the same semiconductor material. Mohapatra [2] reported values of 5×10^{-9} cm^2/s for lithium diffusion in WO_3. On the other hand, Green[3] reported values of 4×10^{-13} cm^2/s. Green also proposed an alternative value of 6×10^{-16} cm^2/s, which was obtained by assuming that the lithium diffusion along grain boundaries occurs very rapidly compared to the time scale of bulk diffusion into the grains. Kanamura et al.[4] and Ottaviani et al.[5] reported values for the lithium insertion in TiO_2 (anatase) of 1.81×10^{-13} cm^2/s (sputtered sample) and 3.7×10^{-10} cm^2/s (sample prepared from commercially available powder). The concept of fast diffusion into grain boundaries or surface roughness was used to explain the results. An interesting study was performed by Cantão et al.[6] These workers investigated lithium insertion in sputtered TiO_2 (crystal structure unspecified). Essentially, they found that the diffusion coefficient increased over almost 3 orders of magnitude if the film thickness was increased. They also observed that the diffusion process was limited in length, which was determined to 11 nm for all film thicknesses. Since the diffusion length was constant, they concluded that the intercalation process was restricted to the width of the accumulation layer. Their interpretation might be correct; nevertheless, their results might also be explained with the concept of inner electrode area. Using this interpretation, a constant diffusion length of 11 nm could then be identified as the effective radius of the particles produced during the sputtering process. (The particle size was not specified.)

Other factors than the total active electrode area influence on the observed rate of intercalation. Weppner et al.[7] developed electrochemical methods to determine chemical diffusion coefficients for insertion electrodes. These models highlight that the motions of the electrons and the inserted ions are coupled and show the same transport rate because of electroneutrality. Thus, the chemical diffusion coefficient obtained from an electrochemical experiment may vary over several orders of magnitude depending on parameters such as diffusivities, mobilities, stoichiometries, doping densities, and activities.

In this paper we compare the electrochemical characteristics of Li^+ ion insertion in porous and compact anatase. The porous anatase samples consisted of the same open framework that has been used successfully in the development of dye-sensitized solar cells[8] and batteries[9,10] by Grätzel and co-workers. The fact that the electrolyte contacts the inner surface of these electrodes is well established.[11,12] The object was to compare the chemical diffusion coefficients for electrodes in which the electrolyte is in contact with each grain in the entire electrode with those of compact electrodes, where the "inner area" (presumably) is available only by diffusion along grain boundaries. The fact that the electrolyte enters the cavities in the nanoporous electrodes also affords a simple way of demonstrating the effects caused by porosity.

2. Experimental Section

Preparation and Characterization of Electrodes. Two different types of TiO_2 (anatase) electrodes were used in this work, i.e., nanoporous (NP) electrodes and chemical vapor

* Authors to whom correspondence should be addressed.
[⊗] Abstract published in *Advance ACS Abstracts,* August 15, 1997.

S1089-5647(97)00489-6 CCC: $14.00

deposited (CVD) electrodes. The NP films were produced by deposition of a colloidal TiO_2 solution with a glass rod on a conducting glass support (F-doped SnO_2; sheet resistance 8 Ω/□).[13] The preparation of the colloidal TiO_2 solution has been described elsewhere.[14] Briefly, titanium isopropoxide was hydrolyzed in nitric acid (8 h at $T = 80$ °C and pH = 1) and autoclaved at 200 °C (12 h) to yield small anatase colloids. Spin coating was used to obtain thinner NP films (<1 μm). All electrodes used in this study were fired in a hot air gun at 450 °C for 30 min. The projected area, the film thickness, and the porosity of the NP electrodes were determined carefully as described earlier.[13] The projected area was typically around 0.5 cm^2, and the porosity $\boldsymbol{P}$ (percentage of voids) was 64 ± 3%, as measured on 10 nanoporous samples of different thicknesses, showing that the films were smooth and homogeneous. The inner area of the sintered nanoporous samples was determined by the equation[15]

$$A_{tot} = 3V_{tot}(1 - P)/r \quad (1)$$

where A_{tot} is the inner area of the nanoporous electrode, V_{tot} is the film volume, and r is the average radius of the anatase particles in the NP film and is taken as 4 nm. Equation 1 assumes that the particles are monodisperse and spherical. Kavan et al.[15] showed in a BET and electrochemical study on 10 different anatase powders/films that the inner area in sintered films might be reduced up to ∼50% compared to the corresponding powders (especially for small and agglomerated particles). The error occurs because the pores in the agglomerated particles disappear during the heat treatment.

The preparation of the chemical vapor deposited (CVD) films followed the procedure described earlier,[16], except that the amount of injected precursor (tetrakis(isopropoxy)titanium) was 0.5 mL. The thickness of the CVD samples was 90 nm as measured by profilometry (Tencor Alpha Step). The porosity of the CVD samples could not be determined. The structure characterization was performed by a Siemens D-5000 diffractometer, showing that all NP and CVD samples consisted of pure anatase. Comparison of the intensity of the peaks indicated a texture effect with predominance to the {101} planes (for both CVD and nanoporous films). The average particle size for the sintered nanoporous electrodes was determined to 7 nm (as obtained from the X-ray diffractogram using Scherrers formula) and 8 nm as determined from TEM pictures on the unsintered colloidal TiO_2 solution. The average particle size in the CVD sample was determined to 33 nm from X-ray measurements.

Electrolyte. The electrolyte solution in all experiments consisted of 2 M $LiClO_4$ in acetonitrile unless otherwise stated. The solvent was prepared from anhydrous acetonitrile, supplied by Aldrich (initial water content <50 ppm), which was subsequently statically dried for several weeks over activated 3 Å molecular sieves (vacuum at 350 °C, 48 h). Anhydrous $LiClO_4$ (Aldrich) with an initial water content <1% was vacuum-dried (180 °C, 48 h) and then mixed with the solvent in a glovebox and stored in "Sure Seal" bottles (Aldrich) under an argon atmosphere. To further lower the concentration of electron acceptors like trace water or other impurities in the electrolyte, 0.1% Li metal was added to the solution. The TiO_2 electrodes were never in contact with the Li metal. All chemicals used were of reagent grade.

Electrochemical Measurements. The electrochemistry was performed using a three-electrode system connected to a multichannel ECO Chemie Autolab/GPES electrochemical interface. For the electrochemistry a thermostatically controlled sealed Metrohm glass vessel was used. The vessel was dried overnight at 110 °C and purged for several hours with dried argon together with the mounted electrodes before the electrolyte was added. Electrolyte (100 mL) was injected into the chamber using Omnifit Teflon tubings with connections for chromatography. The counter electrode consisted of glassy carbon and was enclosed with a glass frit to avoid the influence of reaction products. The reference electrode was a Ag/AgCl in saturated LiCl (Merck) in anhydrous acetonitrile. The potential of this electrode was −0.05 V from that of a Ag/AgCl in saturated LiCl in ethanol. The LiCl was dried at 200 °C for several weeks before use. All potentials are referred to the Ag/AgCl electrode. The potential variation of the reference electrode between 25 and 60 °C was less than 3 mV. The atmosphere in the cell compartment was purged with a slight overpressure of argon. The initial water content in the argon was <5 ppm, and the gas was predried in a glass column (40 cm) containing activated molecular sieves (4 Å), before the inlet to the cell compartment. To avoid the buildup of a diffusion layer outside the TiO_2 films, the electrolyte solution was heavily stirred with a magnetic stirrer during all experiments. A Pt electrode was used in situ as an indicator of the relative water content. By cycling the Pt electrode between 0 and −1.5 V at 20 mV/s, it was found that a residual current (mainly capacitive, no redox peaks) of 1−5 $\mu A/cm^2$ gave excellent lithium insertion/extraction reversibility in the TiO_2. The current from the naked conducting glass was even smaller, 300−700 nA/cm^2. Each electrode was preheated at 450 °C in air for 10 min and transferred directly to the electrochemical cell in an desiccator. Before any potential steps were performed, the nanoporous electrodes were cycled (20 mV/s) ∼20 times between 0 and −1.5 V to remove adsorbed water on the surface of the electrodes.[11] The first scan yielded typically an extraction−insertion ratio between 97 and 99%. The subsequent scans yielded ratios above 99%. The cathodic steps were performed after keeping the electrode at a potential of 0 V for 30 min. The anodic steps were analogously performed after keeping the electrode at −1.5 V for 30 min.

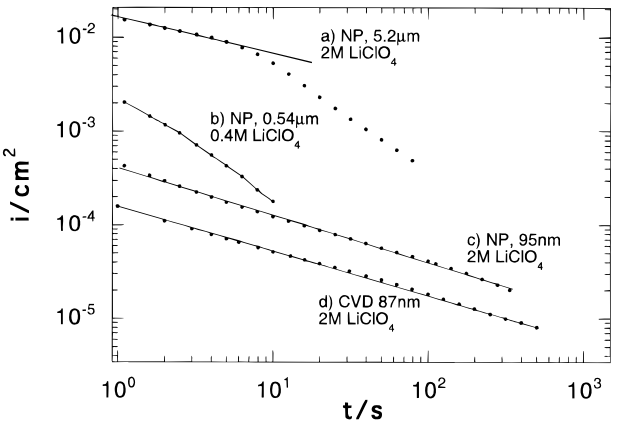

Figure 1. Currents for nanoporous electrodes of different thicknesses (a−c) and a CVD sample (d) after a potential step from 0 to −1.3 V. The electrode thickness d, and concentration of $LiClO_4$ in each experiment are indicated in the figure. $T = 45$ °C.

3. Results and Discussion

Film Thickness Dependence on the Current. Potential steps were performed between 0 and −1.3 V on a CVD sample (d) and nanoporous (NP) films with different thicknesses (a−c). The typical response is shown in Figure 1. The currents are normalized with respect to the back contact area and plotted vs time on a log−log scale. Comparing the initial currents from the NP electrodes, (a) and (c), it can be seen that the curves are parallel with magnitudes scaling with the film thickness. The CVD film (d) exhibits the lowest current. The slopes of all

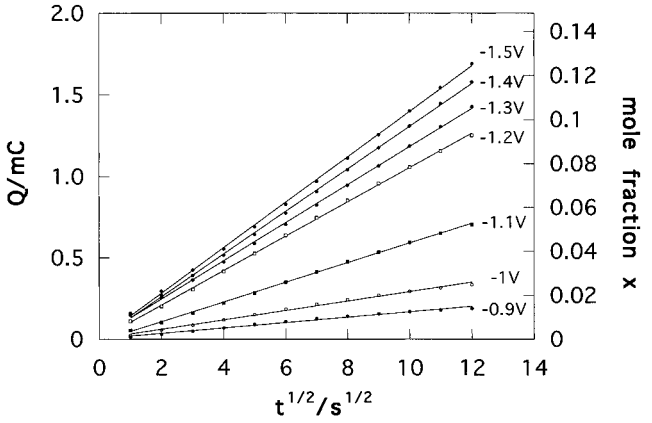

Figure 2. Integrated charge at different potential steps vs $t^{1/2}$ for a CVD sample, $d = 90$ nm. $T = 45$ °C.

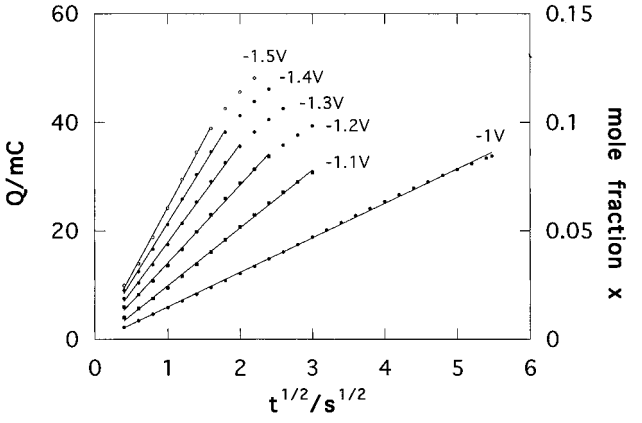

Figure 3. Integrated charge vs $t^{1/2}$ at different cathodic potential steps for a nanoporous electrode, $d = 2.20$ μm. $T = 45$ °C.

initial currents (except (b)) have a value of -0.5 ± 0.05. However, while a slope of -0.5 is retained for several hundreds of seconds for the thinner NP film (c), the thicker nanoporous electrode (a) falls off from this dependence after about 10 s. The integrated charge during the first 10 s corresponds roughly to the amount of Li^+ ions in the cavities of the nanoporous films. Curve b shows the response from a nanoporous electrode using an electrolyte concentration of 0.4 M. The magnitude of the initial current scales roughly with the film thickness; however, the decay is much sharper, and the initial slope of -0.5 is never attained.

The low current from the CVD sample (d) is due to the small electroactive electrode area. The linear relationship between the initial currents and the film thickness for the NP films (a−c) shows that the currents are directly proportional to the volume of the electrode, which in turn assures that the entire inner electrode area is homogeneously electroactive. Hence, the potential drop across the nanoporous system is small, and the electric potential is mainly the same from the back contact and throughout the film. Thus, the electrical potential at the surface of each particle in the film corresponds to that desired by the potentiostat. A slope of -0.5 is expected for a diffusion-limited process[17] if the current after a potential step is monitored on a log−log scale. Changing the film thickness or electrolyte concentration illustrates unique properties of the nanoporous electrodes. At higher film thicknesses (a) depletion of electrolyte in the pores becomes a limiting factor. This is seen as a sharp deviation from the diffusional current after about 10 s. The same course is observed at a much earlier stage if the electrolyte concentration is lowered; see curve b.

Potential Dependence on the Current. The integrated charge, Q, was plotted vs the square root of time, $t^{1/2}$, at various cathodic potential steps for a CVD sample (Figure 2). The initial potential was 0 V. It can be seen that the charge is directly proportional to the square root of time and that the slopes increase dramatically down to -1.2 V. The highest inserted mole fraction during the time period of the experiment was 0.13, as determined by the ratio between the number of injected electrons and the number of titanium atoms in the electrode.

Double injection of electrons and charge-compensating Li^+ ions into anatase leads to the formation of Ti^{3+} states.[18,19] The same characteristic has been reported for proton intercalation in anatase (see ref 20 and references therein). The increasing slope at more negative steps suggests therefore that the surface concentration of Ti^{3+} states is potential dependent; i.e., higher Ti^{3+} surface concentrations are obtained at more negative potentials. Accordingly, the observed current, which is limited by diffusion of Li^+ ions in the TiO_2 lattice, is expected to increase at more negative potential steps (due to the larger concentration gradient). The small change of the slope of the curves below -1.2 V indicates that the surface layer of the electrode is nearly saturated with Ti^{3+} ions.

Figure 3 shows the potential dependence on the rate of Li^+ insertion in a 2.2 μm nanoporous electrode. It can be seen that the behavior of the nanoporous electrode and the CVD sample is essentially the same. However, the initial diffusional parts of the curves in Figure 3 are substantially prolonged at less negative potential steps. The highest inserted mole fractions are around 10%.

The conclusion is that, at less negative steps, the surface concentration of Ti^{3+} states is lower, implying a slower consumption (i.e., slower depletion) of Li^+ ions in the cavities of the nanoporous electrode. This feature is not observed for the CVD sample.

Diffusion Coefficient. To determine the chemical diffusion coefficient for insertion and extraction of lithium, we make use of the equation describing a chronocoulometric response under diffusion-limited conditions[17]

$$Q = 2n\pi^{-1/2}FAD^{1/2}C^*t^{1/2} + Q_{dl} + nFA\Gamma \qquad (2)$$

where Q is the integrated charge, A is the electroactive electrode area, D is the chemical diffusion coefficient,[7,21] C^* is the surface concentration, Q_{dl} arises because of double-layer charging, and Γ is the concentration of adsorbed species taking part in the faradaic reaction. The intercept in a Q vs $t^{1/2}$ plot at $t = 0$ can thus be interpreted as the sum of (i) the accumulated charge caused by the non-faradaic Helmoltz layer redistribution (to charge compensate for the change in electron concentration in TiO_2) and (ii) the faradaic reduction of the Ti^{4+} states which is assumed to occur instantaneously at those positions at the TiO_2 surface where the charge-compensating ions are adsorbed (see below). Equation 2 is derived for the case of linear semiinfinite diffusion. Therefore, we assume that the bulk Ti ions in the center of the particles constituting the NP electrode, and the Ti ions close to the back contact of the CVD sample, are not affected during the time period of the experiment. The indicated mole fractions in Figure 2 and Figure 3 shows that this assumption is reasonable (about 13% for the CVD electrode and 10% for the nanoporous film). In addition, the observed $t^{1/2}$ dependence would not be obtained if the semiinfinite condition was not satisfied; cf. ref 22. Since the injected charge during the analyzing time is small, only the surface atomic layers of the particles in the NP electrode are affected, and spherical bulk diffusion into the grains is therefore neglected.

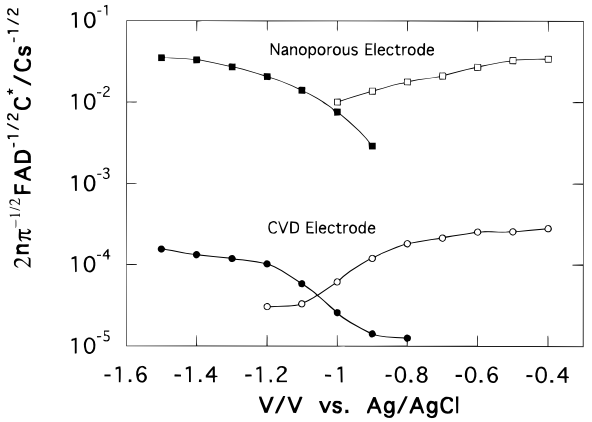

Figure 4. Obtained slopes from $Q-t^{1/2}$ plots for insertion and extraction vs the corresponding potential steps. $T = 45$ °C.

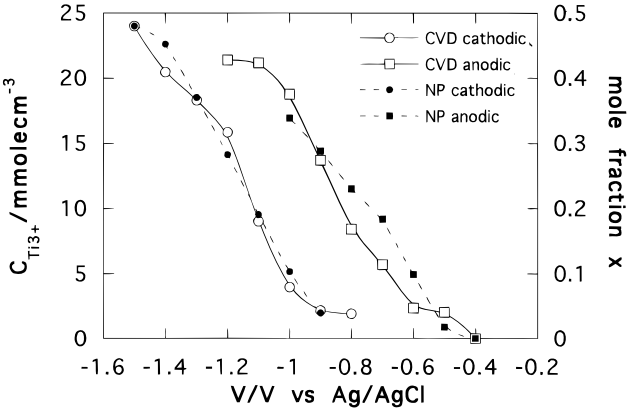

Figure 5. Calculated surface concentrations of Ti^{3+} states at cathodic and anodic potential steps. $T = 45$ °C.

The obtained slopes from Q-$t^{1/2}$ plots for insertion and extraction for a NP electrode and a CVD sample are plotted vs the step potential in Figure 4 The slope is identified as $2n\pi^{-1/2}FAD^{1/2}C^*$, according to eq 2. Comparing the slopes for insertion, it can be seen that the curves have similar shapes. The same feature is true for extraction; however, the shapes are merely the mirror image of those for insertion. The slopes are mainly constant below −1.2 V (cathodic steps) and more positive than −0.6 V (anodic steps). The slopes are typically orders of magnitudes larger for the nanoporous film compared to the CVD electrode.

The conclusion is that lithium insertion into the nanoporous film behaves similarly to that of the compact bulk sample. The large difference in the slopes for the nanoporous film and CVD sample is an obvious consequence of the large difference in active electrode area.

For the insertion process, we consider that the TiO_2 lattice is completely oxidized initially (at 0 V). Next, we assume that the surface of the particles in the porous electrode and the surface of the CVD sample is completely saturated with Ti^{3+} states after a sufficiently negative potential step. Examining Figure 4, this occurs when the plateau is reached at potentials more negative than −1.2 V. The useful potential range for organic electrolytes permits maximum mole fractions typically around 0.5.[11,15,23,24] (Although at stronger overpotentials (−2 V), i.e., using electrochemically more stable gel electrolytes or powerful reducing agents like tertbutyllithium, mole fractions of 0.7−0.8 can be achieved.[23,24]) Thus, we assume that the surface concentration of Ti^{3+} after the cathodic step to a sufficiently negative potential corresponds to $x = 0.5$, i.e., 24×10^{-3} mol/cm^3.[12] The analysis for the lithium extraction is just the opposite to that of the insertion. Initially after keeping the electrode at −1.5 V for 30 min, the concentration of Ti^{4+} is set to zero since all electrochemically available Ti^{4+} states are assumed to be reduced. After an anodic potential step more positive than −0.6 V, we assume that the surface concentration of Ti^{4+} is $x = 0.5$, analogous to the insertion process. Using the slopes for the insertion from 0 to −1.5 V and extraction from −1.5 to −0.5 V, for the nanoporous film, gives diffusions coefficients of 3×10^{-17} cm^2/s (insertion) and 1×10^{-16} cm^2/s (extraction). Assuming ∼50% area loss during sintering[15] increases the diffusion coefficient for the NP electrode by a factor of 4 (due to the square dependence in eq 2). The corresponding values for the CVD sample are 9×10^{-15} cm^2/s (insertion) and 4×10^{-14} cm^2/s (extraction). The effect of the grain boundaries in the CVD sample may be considered: The CVD sample was 90 nm thick and consisted thus of roughly three layers of closely packed 30 nm particles. Assuming that the CVD sample is nonporous (with $P = 0$, in eq 1) such that Li^+ ion diffusion only can occur along the grain boundaries gives a chemical diffusion coefficient 6×10^{-17} cm^2/s, i.e., 300 times lower.

If the inner area of the nanoporous and CVD sample is considered, similar chemical diffusion coefficients are obtained. This indicates that the diffusion of Li^+ ions along the grain boundaries in the CVD sample might be much faster than the bulk diffusion into the grains. Unfortunately, the film thickness of the CVD samples could not be varied, and therefore we do not know whether the inner area of the CVD samples was electrochemically active during the experiments. However, Cãntao et al.[6] showed that the diffusion coefficients for Li^+ insertion in TiO_2 might vary over several orders of magnitude if the thicknesses of the sputtered samples is changed, indicating that the inner area in denser electrodes might be of importance. Kavan et al. reported relatively high chemical diffusion coefficients around 10^{-13} cm^2/s for lithium intercalation in small single crystals of anatase (10 mm^3) using chronoamperometry. The specimens were doped by reduction in hydrogen (500−600 °C) and contained also Al (0.2−0.5%). In comparison with this study, their results indicate that impurity or vacancy doping offers a way to increase the chemical diffusion constant of insertion and extraction of lithium in anatase.

We note that the magnitude of the diffusion coefficient for the nanoporous films obtained from chronoamperometry in this study agree essentially with that from voltammetry in part 2 and with XPS measurements,[18] where the chemical diffusion coefficient was determined by measuring the Ti^{3+} concentration in the particles in the outer layers of a NP electrode.

Surface Concentration of Ti^{3+}. By assuming that the obtained chemical diffusion constant is independent of the magnitude of the surface concentration, we can estimate the surface concentration of Ti^{3+} at different potentials by inserting the diffusion constant and the slopes at various potential steps into eq 2. The results are shown in Figure 5. The curves for insertion and extraction are similar and have the sigmoidal shape of a conventional titration curve. However, the curves for insertion and extraction do not coincide.

Under the given assumptions, Figure 5 indicates how the surface concentration varies with potential for cathodic and anodic potential steps. The assumptions may lead to errors in the calculated surface concentration of Ti^{3+}, but the potential shift for the cathodic and anodic potential steps is significant. The hysteresis (potential shift) for insertion and extraction suggests that the surface concentration depends on the conditions at the initial state before the potential step is made. Thus,

applying a step to e.g. −0.9 V results in different surface concentrations depending on whether the step is made from 0 V (where only TiO_2 is present) or −1.5 V (where presumably only $Li_{0.5}TiO_2$ is present). We explain the hysteresis as due to the sluggishness in reducing Ti^{4+} states or oxidizing Ti^{3+} states at the surface of the particles. Thus, a significant overpotential is needed to reach the limiting cathodic and anodic currents, and the kinetics of the system cannot be considered Nernstian but rather irreversible.[25] Since the potential shift between the curves for insertion and extraction is mainly constant, about 0.25 V, and therefore independent of the magnitude of the currents drawn at different steps, we exclude again the presence of a potential drop across the nanoporous network.

It has been suggested[23,24] that a two-phase equilibrium (TiO_2 and Li_xTiO_2) is present at $0 < x < 0.5$, leading to a potential-independent *x*-value. Hence, for a two-phase system one would not expect a dependence of the current on the overpotential.[1] However, the observed potential-controlled rate of the redox reactions in our experiments suggests that lithium intercalation in anatase, kinetically, exhibits the behavior of a one-phase reaction. The explanation may be that a two-phase equilibrium is not reached within the period of the transient experiment, because of the low mobility of Li^+ in the TiO_2.[1]

Capacitance and Surface Concentration of Adsorbed Species. The intercepts (recognized as the two last terms in eq 2) from cathodic *Q* vs $t^{1/2}$ curves for two nanoporous electrodes (0.23 and 5.20 μm) were plotted as a function of the step potential (Figure 6). The intercepts were normalized with respect to the inner electrode area. The intercept increases when the step is performed to a more negative potential. The following interpretation is made: During the early time stages, i.e., some hundreds of milliseconds, we assume that the current is dominated by double-layer charging and electrochemical surface reactions due to adsorbed ions (see above). Thus, the mass transport of Li^+ ions inside the TiO_2 lattice is neglected. The rationale for this assumption is based on our observation that the diffusion constant of Li^+ in nanoporous anatase is very small. We also assume that the potential drop occurs mainly across the Helmholtz layer.[26] If the double-layer capacitance can be assumed constant in the examined potential range, then the non-faradaic charging current is[27] for the potential step from

$$Q_{dl} = C_{dl}(E_j - E_i) \tag{3}$$

the initial potential, E_i (0 V), to the potential E_j. If E_j is made more negative than the peak potential (−1.1 V), then all of the adsorbed species at the initial potential can be assumed to be reduced. The total charge passed during the potential step is then[27]

$$Q = Q_{dl} + Q_{ads} = C_{dl}(E_j - E_i) + nF\Gamma \tag{4}$$

Thus, a plot of *Q* vs $E_j - E_i$ yields an intercept of $nF\Gamma$ and a slope of C_{dl}. The obtained curves in Figure 6 are roughly linear. The onset potential for the charge is −1 V. The calculated values for the capacitance and the surface concentration of adsorbed species for the two electrodes are $C_{dl} = 35 \pm 5$ μF/cm^2 and Γ (at 0 V) $= (2.0 \pm 0.3) \times 10^{14}$/cm^2. The obtained adsorbate concentration can be attributed to several matters: (i) surface-adsorbed Li^+ ions, (ii) hydroxylic groups on the anatase surface, or (iii) traps (other than (i) and (ii)). It has been observed that oxides in protic electrolytes exhibit pseudocapacitance due to adsorbed hydroxylic groups (ii). The effect consists of faradaic electron transfer to those surface metal ions where the charge-compensating H^+ ions are adsorbed. It has also been shown that the adsorbed protons on anatase particles

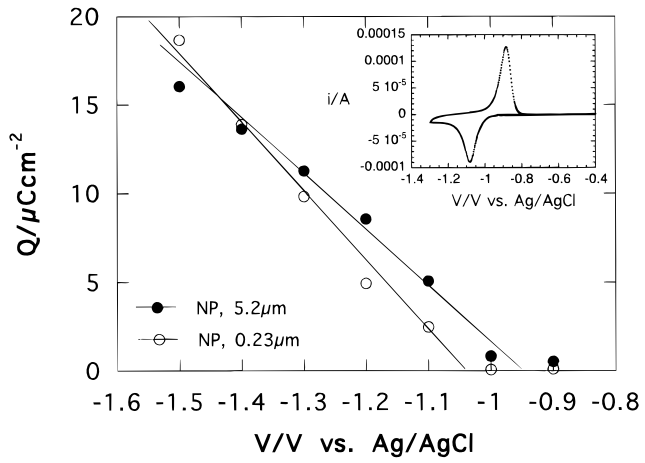

Figure 6. Intercepts from $Q-t^{1/2}$ plots of two NP electrodes of different thicknesses as a function of the corresponding negative potential steps. The inset shows a cyclic voltammogram at 0.1 mV/s. $T = 45$ °C.

can be exchanged with metal ions.[28] (This fact can be used to calculate the amount of surface hydroxylic groups.) The obtained values of the capacitance and adsorbate concentration are very similar to those for hydroxylated anatase (surface with a monolayer coverage), $\Gamma_{OH} = (1 - 5) \times 10^{15}$/cm^2 and $C_{dl} = 16 - 80$ μF/cm^2.[12] However, in this study the concentration of Li^+ is high, 2 M, and the water concentration in the aprotic acetonitrile is very low (since the current from the Pt electrode is very low and the insertion/extraction ratio from cyclic voltammetry is virtually unity; see Experimental Section and part II). Therefore, we propose that the protonic adsorption equilibrium is replaced by a similar equilibrium for Li^+ ions, as discussed previously by Redmond et al.[29] The idea is justified since the charge in Figure 6 start to increase at −1 V, i.e., the same potential as the "on-set" for lithium intercalation (see the CV inset in Figure 6). Additionally, the onset (as measured optically) for the reduction of nanoporous anatase in dry acetonitrile is shifted to very low values, −2 V, in the absence of Li^+ ions.[29]

We cannot perfectly exclude the possibility that the adsorbate concentration measures the density of traps (crystal defects) in the particles. Using this interpretation, one could speculate that the traps in the particles are empty (oxidized) at the initial potential, 0 V. Furthermore, after the negative potential step, the electrons injected into the network would then in the early time stages reduce the traps in the particles in a similar way to the behavior of pseudocapacitance. Thus, we cannot distinguish electron capture by intrinsic defects, i.e., trap filling, from surface adsorption of cations from the solution.

Temperature Dependence. The cathodic $Q-t^{1/2}$ plots for a nanoporous electrode (a) and a CVD sample (b) are displayed in Figure 7 The steps were made between 0 and −1.3 V. The increase of the currents at higher temperatures shows that the diffusion of Li^+ ions in the anatase lattice is thermally activated. The obtained slopes at several temperatures were used to calculate the corresponding chemical diffusion coefficients according to the method described above. The cathodic and anodic potential steps were performed from 0 to −1.3 V and −1.5 to −0.5 V. The activation energy for intercalation and deintercalation was obtained using the relation

$$D = D_0 e^{-E_a/kT} \tag{5}$$

where D_0 is the preexponential factor, E_a is the activation energy, *k* is the Boltzmann constant, and *T* is the absolute temperature.

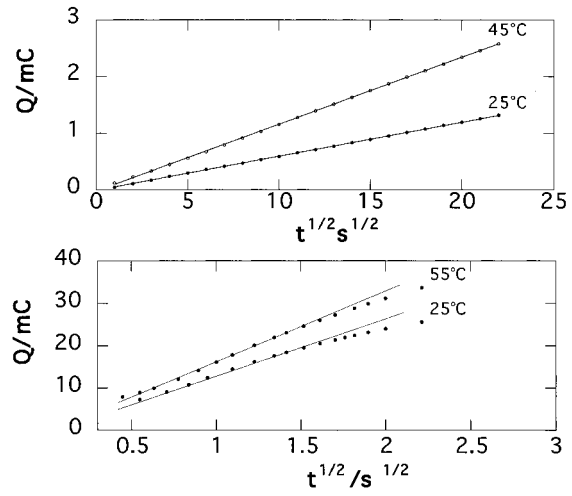

Figure 7. Currents of a nanoporous electrode following a potential step from 0 to −1.3 V at 25 and 55 °C (a). The current response of a CVD electrode after a potential step from 0 to −1.3 V at 25 and 45 °C (b).

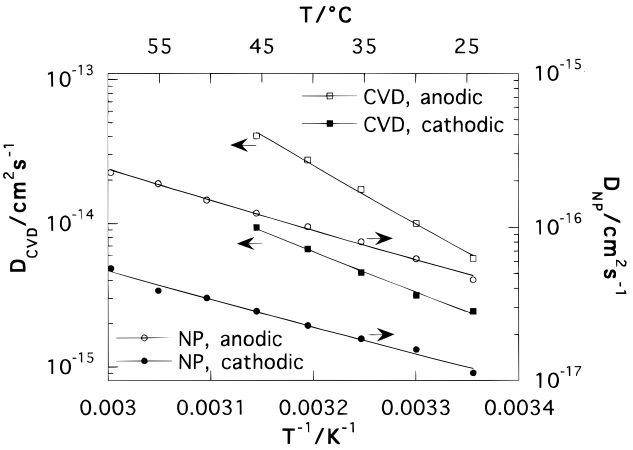

Figure 8. Inverse temperature dependence of the logarithm of the chemical diffusion coefficient for insertion and extraction in a CVD sample and a NP electrode.

Figure 8 shows the logarithm of the diffusion coefficients vs the inverse temperature. The activation energy was determined to 0.35 and 0.38 eV for insertion and extraction in the nanoporous electrode. The corresponding values for the CVD sample were 0.54 and 0.78 eV.

The activation energies for the CVD electrode are higher than those of the nanoporous electrode, indicating that insertion and extraction of lithium in nanoporous TiO_2 electrodes are favored. The explanation might be that the electrostatic screening of the inserted electrons and Li^+ ions is improved in the nanoporous system since each particle ($d = 8$ nm), is surrounded by the charge-compensating electrolyte. Other authors have reported values around 0.5[30] or 0.5−0.7 eV[31] for the insertion of lithium in fluorine-doped sputtered TiO_2 (crystal structure not determined). Differences in activation energies have been observed for crystalline and X-ray amorphous films of WO_3,[32] where the amorphous films exhibited lower activation energies. The discrepancy was explained by different stoichiometries or by different transport mechanisms of the guest species.

4. Conclusions

The effect of inner electrode area and porosity of anatase on the rate of Li^+ ion intercalation was demonstrated. The observed rate of electrochemical insertion and extraction of Li^+ ions in nanoporous electrodes was directly proportional to the inner electrode area. The chemical diffusion coefficients for compact and porous electrodes were similar if the inner area of the electrodes was taken into account. Mass transport of the electrolyte in the pores is a rate-limiting factor for thicker nanoporous films (a few micrometers). The potential dependence on the rate of insertion and extraction shows that the reduction of Ti^{4+} and oxidation of Ti^{3+} are kinetically hindered. The potential dependence on the integrated charges at the early time stages indicates the presence of adsorbed species. The adsorbate concentration (proposed as being due to adsorbed Li^+ ions) corresponded to almost a monolayer. The activation energies was higher for the CVD sample compared to the nanoporous films, indicating that lithium intercalation in nanoporous anatase is favorable.

Acknowledgment. This work was supported by the Swedish Research Council for Engineering Sciences (TFR), the Commission of the European Community Joule II program, and the Swedish National Research Council (NFR).

References and Notes

(1) Bruce, P. G. *Solid State Electrochemistry*; Press Syndicate of the University of Cambridge: Cambridge, 1995.
(2) Mohapatra, S. K. *J. Electrochem. Soc.* **1978**, *125*, 284−288.
(3) Green, M. *Thin Solid Films* **1978**, *50*, 145−150.
(4) Kanamura, K.; Yuasa, K.; Takehara, Z. *J. Power Sources* **1987**, *20*, 127−134.
(5) Ottaviani, M.; Panero, S.; Morzilli, S.; Scrosati, B. *Solid State Ionics* **1986**, *20*, 197−202.
(6) Cantão, M. P.; Cisneros, J. I.; Torresi, R. M. *J. Phys. Chem.* **1994**, *98*, 4865−4869.
(7) Weppner, W.; Huggins, R. A. *J. Electrochem. Soc.* **1977**, *124*, 1569−1578.
(8) Nazeeruddin, M. K.; Kay, A.; Rodicio, I.; Humphry, B. R.; Mueller, E.; Liska, P.; Vlachopoulos, N.; Grätzel, M. *J. Am. Chem. Soc.* **1993**, *115*, 6382−90.
(9) Huang, S.-Y.; Kavan, L.; Kay, A.; Grätzel, M. *J. Act. Passive Electron. Compon.*, in press.
(10) Huang, S. Y.; Kavan, L.; Exnar, I.; Grätzel, M. *J. Electrochem. Soc.* **1995**, *142*, 142−144.
(11) Kavan, L.; Kratochilová, K.; Grätzel, M. *J. Electroanal. Chem.* **1995**, *394*, 93−102.
(12) Kavan, L.; Grätzel, M.; Gilbert, S. E.; Klemenz, C.; Scheel, H. J. *J. Am. Chem. Soc.* **1996**, *118*, 6716−6723.
(13) Lindström, H.; Rensmo, H.; Södergren, S.; Solbrand, A.; Lindquist, S.-E. *J. Phys. Chem.* **1996**, *100*, 3084−3088.
(14) O'Regan, B.; Grätzel, M. *Nature (London)* **1991**, *353*, 737−40.
(15) Kavan, L.; Grätzel, M.; Rathousky, J.; Zukal, A. *J. Electrochem. Soc.* **1996**, *143*, 394−400.
(16) Hagfeldt, A.; Vlachopoulos, N.; Grätzel, M. *J. Electrochem. Soc.* **1994**, *141*, L82.
(17) Bard, A. J.; Faulkner, L. R. *Electrochemical Methods*: *Fundamentals and Applications*; John Wiley & Sons: New York, 1980.
(18) Södergren, S.; Rensmo, H.; Lindström, H.; Hagfeldt, A.; Lindquist, S.-E.; Siegbahn, H. To be published.
(19) Stashans, A.; Lunell, S.; Bergström, R.; Hagfeldt, A.; Lindquist, S.-E. *Phys. Rev. B* **1996**, *53*.
(20) Cao, F.; Oskam, G.; Searson, C.; Stipkala, J. M.; Heimer, T. A.; Meyer, G. J. *J. Phys. Chem.* **1995**, *99*, 11974−11980.
(21) The chemical diffusion coefficient is obtained if only the concentration gradient is considered, i.e., the activity gradient is not taken into account. Also see ref 1.
(22) Crank, J. *Mathematics of Diffusion*; Oxford University Press: London, 1956.
(23) Murphy, D. W.; Greenblatt, M.; Zahurak, S. M.; Cava, R. J.; Waszczak, J. V.; Hull, G. W.; Hutton, R. S. *Rev. Chim. Miner.* **1982**, *19*, 441.
(24) Zachau-Christiansen, B.; West, T.; Jacobsen, T. a. A., S. *Solid State Ionics* **1988**, *28*−30, 1176.
(25) In part 2 the standard rate constant was determined to $\sim 10^{-10}$ cm/s, showing that the reduction and oxidation of Ti ions at the surface are very sluggish and can be classified irreversible.
(26) In part 2 the value of the determined value of the transfer coefficient is close to 0.5 as for metals.

(27) Stankowich, M. T.; Bard, A. J. *J. Electroctroanal. Chem.* **1978**, *86*, 189−199.
(28) Zang, L.; Liu, C.-Y.; Ren, X.-M. *J. Chem. Soc., Chem. Commun.* **1994**, 1865.
(29) Redmond, G.; Fitzmaurice, D. *J. Phys. Chem.* **1993**, *97*, 1246−1430.
(30) Stromme, M.; Gutarra, A.; Niklasson, G.; Granqvist, C. G. *J. Appl. Phys.* **1995**, *79*, 3749−3757.
(31) Stromme Mattsson, M.; Niklasson, G. A.; Granqvist, C. G. *J. Appl. Phys.*, in press.
(32) Randin, J.-P.; Viennet, R. *J. Electrochem. Soc.* **1982**, *129*, 2349−2354.